NACA RM E54D12

NACA

RESEARCH MEMORANDUM

FORCED-CONVECTION HEAT-TRANSFER AND PRESSURE-DROP CHARACTERISTICS OF A CLOSELY SPACED WIRE MATRIX

By Louis Gedeon and Milton D. Grele

Lewis Flight Propulsion Laboratory
Cleveland, Ohio

NATIONAL ADVISORY COMMITTEE
FOR AERONAUTICS

WASHINGTON
August 13, 1954
Declassified October 16, 1961

1P

NACA RM E54D12

NATIONAL ADVISORY COMMITTEE FOR AERONAUTICS

RESEARCH MEMORANDUM

FORCED-CONVECTION HEAT-TRANSFER AND PRESSURE-DROP CHARACTERISTICS OF A CLOSELY SPACED WIRE MATRIX

By Louis Gedeon and Milton D. Grele

3250

SUMMARY

An investigation was made of the forced-convection heat-transfer and pressure-drop characteristics of a staggered closely spaced 0.020-inch wire metal-to-air heat exchanger. Eight wire banks were electrically heated, and the range of variables included bulk Reynolds numbers based on wire diameter and maximum velocity, from 82 to 1900, average wire temperatures up to 1109° R, and heat flux densities up to 84,000 Btu per hour per square foot. An attempt was made to correlate the isothermal wire-screen pressure-drop data of various investigators.

The heat-transfer data based on the physical properties of air at the film temperature resulted in a good correlation throughout the range of Reynolds numbers investigated. The data were evaluated on the basis of free-flow factor as well as porosity, which is a measure of the volume of void within the wire matrix. The scatter of the data was reduced by means of a modified correlation method in which the product of the air density at the film temperature and the bulk upstream velocity was substituted for the conventional mass flow per unit cross-sectional area in the Reynolds number.

Isothermal wire-screen pressure-drop data of various investigators were cross-plotted to determine a correlation of drag coefficient and free-flow factor. The result obtained was applied to the data of the present investigation.

INTRODUCTION

The use of an air-cooled nuclear reactor as a power source for propulsion of aircraft is of considerable current interest. Inasmuch as air is a relatively poor heat-transfer medium, it is desirable to incorporate as much heat-transfer surface into such a reactor as is feasible. To do this, fine-grained heat-transfer matrices are required. One possible matrix consists of banks of small wires, or screens, in which the heat is generated, and across which the cooling air is passed. Forced-convection heat-transfer data for such fine-grained configurations are sparse, and what data are available have been obtained by transient techniques at extremely low heat-flux densities. All available pressure-drop data were obtained for isothermal flow.

An experimental investigation has been undertaken at the NACA Lewis laboratory to augment knowledge on the heat-transfer and friction characteristics of wire matrices. As a part of this general program, an investigation has been conducted with air flowing across eight banks of closely spaced electrically heated 0.020-inch-diameter Nichrome V tubes. The range of variables included bulk Reynolds numbers based on wire diameter and maximum velocity, from 82 to 1900, average wire temperatures up to 1109° R, and heat-flux densities up to 84,000 Btu per hour per square foot.

APPARATUS

Air system. - A photograph and a schematic diagram of the test setup are shown in figure 1. Air at a pressure of 120 pounds per square inch gage is supplied through a surge tank, air cleaner, and a bank of orifices where the flow is measured. From the orifices the air passes through a valve into the inlet duct, through the test channel, across the wire heat exchanger, and is exhausted to the atmosphere.

Heat exchanger. - A photograph, a schematic diagram of the test channel and test heat exchanger, as well as an enlarged photograph of a thermocouple installation are shown in figure 2. The heat exchanger was made up of eight banks of Nichrome V tubes with 0.020- and 0.010-inch outside and inside diameters, respectively. Each bank consisted of 48 tubes with a 0.039-inch spacing between tube centers. The matrix was fabricated to give a staggered tube arrangement with a 0.039-inch spacing between tube bank centers except for a spacing of 0.10 inch between the fourth and fifth banks. The heat-transfer length of each tube was 2 inches, and the test channel dimensions were 2.0 inches high by 1.9 inches wide. The free-flow factor for the matrix was 0.494, and the porosity, which is defined as the volume of matrix voids divided by the total volume of the matrix, was 0.821. Nichrome V tubing was used rather than solid wires so that temperature measurements of the tube could be

made. Chromel-alumel thermocouples were made, from 0.003-inch-diameter wire, by joining the two wires with silver solder. A glass sleeving with an outside diameter of about 0.007 inch was slipped over the thermocouple, and the entire assembly was threaded into the particular Nichrome V tube in which a temperature measurement was desired. The junction was positioned at a predetermined location, and the reading obtained from the thermocouple was considered to be the outside tube wall temperature, inasmuch as calculations showed that the temperature drop through the wall was negligible. The chromel and alumel wires came out at opposite ends of the tube and were fastened to terminal strips. Thirty-two thermocouples were installed in the matrix, located at the positions shown in figure 2.

The Nichrome V tubes were secured to copper header plates which served as a bus bar. The header plates were first drilled to give the desired tube spacing, the tubes were slipped into place, and the entire assembly was silver-soldered together. Electrically the first four banks were connected in parallel, as were the second four banks, and the two sets of four banks were connected in series. To accomplish this, the top header plate was split between the fourth and fifth banks by an electrical insulator. The spacing between the fourth and fifth banks was increased to 0.10 inch to decrease the possibility of a short circuit in the event the tubes began warping at elevated temperatures. To further insure against a short circuit, a small glass tube was used as a spacer and inserted between the fourth and fifth banks. The top header plate was firmly fixed, while the lower header plate was allowed to move as the tubes expanded at elevated temperatures. This was accomplished by making a slip fit of the header plate and the bottom of the flow channel and suspending a weight from the header plate. A totally enclosed box at the bottom of the flow channel housed the weight and the thermocouples that come out of the tubes in the bottom header plate. The thermocouple leads were brought out of the totally enclosed box through a rubber seal. This box was sealed off from the atmosphere and was essentially at the same pressure as the flow channel, and therefore the leakage around the slip fit at the bottom header plate and the bottom of the flow channel was kept at a minimum.

The inlet and outlet air temperatures were measured by thermocouples located approximately 1/4 inch before the first bank and 1/4 inch after the eight bank, respectively. Thermocouple rakes consisting of six open-ball chromel-alumel thermocouples were originally installed to obtain inlet and outlet air temperatures. However, the open-ball thermocouples were found to be affected by radiation from the heated tube banks, and therefore were replaced with a single aspirated chromel-alumel thermocouple at the inlet and outlet side. It was found that a single thermocouple located at the center of the flow duct on the inlet side was representative of the inlet temperature. At the outlet, however, the temperature profile was not uniform, and a temperature survey was obtained by taking measurements at seven transverse positions. The average of the seven readings was taken as the average outlet air temperature. It

should be noted that in figure 2(a), the thermcouple rakes are shown at the exit of the wire banks. The single aspirated thermocouple was used for the test data, but the open-wall thermocouples were never removed and no readings were taken with them. Three static-pressure taps at the inlet and exit were located on the copper bus bar which makes up the top of the flow channel. The pressure taps were located 1/4, 7/8, and $1\frac{1}{4}$ inches from the first and eighth tube banks. The transition from the inlet tank to the test flow channel was a rounded entrance.

Electric system. - Electric power from a 208-volt 60-cycle line was supplied to the test section, as shown in figure 1(b), through two saturable reactors and a power transformer. A voltage regulator controlling the direct-current supply to the reactor maintained close voltage regulation at the primary of the power transformer for any setting (test-section input) of the variable transformer control. The capacity of the electric equipment was 25 kilovolt-amperes at a maximum input of 10 volts across the test section. The power input was read from a calibrated ammeter, voltmeter, and wattmeter.

PROCEDURE

The experimental procedure was as follows: the air flow across the tube banks was set at a minimum desired level, and the power input was adjusted to give the approximate desired average wall temperature. After equilibrium conditions had been reached, all power input, pressure, and temperature readings were recorded. The air flow was then increased, and the power input was increased to maintain the desired tube wall temperature, and the foregoing procedure was repeated. At the high weight flows, considerable wire vibration was observed. Prolonged vibration could have damaged the instrumentation within the tubes; therefore, the data of this investigation were limited to the lower range of Reynolds numbers. The procedure was repeated for three wall temperatures over a range of flow rates.

RESULTS AND DISCUSSION

The basic data obtained in this investigation are listed in tables I and II.

Heat balance. - The heat balance is shown in figure 3, where the total electric heat input Q_p is plotted against the heat transferred to the air Q as determined from the flow rate, specific heat, and increase in total temperature. No heat-loss measurements were taken for the heat exchanger. The solid 45° line is shown to represent the perfect heat-balance condition. It is seen that most of the data fall within the ± 10 percent lines shown dashed.

Tube-wall temperature distribution. - Representative axial tube bank temperatures are shown in figure 4. Each plotted point is an average tube bank temperature. The slight dip at the inlet may be due to the fact that the heat-transfer coefficient is lower for the first bank than for the second bank. A radiation loss from the last bank may be the cause of the slight dip at the exit.

Correlation of Heat-Transfer Coefficients

Heat-transfer coefficients. - Average heat-transfer coefficients were obtained from the following equation (All symbols are defined in the appendix):

$$h = \frac{Wc_{p,b}(T_2 - T_1)}{S(T_s - T_b)}$$

where:

T_1 temperature at inlet of tube matrix

T_2 average of seven thermocouple readings taken at different transverse locations at exit of tube matrix

T_s average wall temperature of tube matrix (obtained by first averaging the thermocouple readings for each individual bank and then averaging the temperature of the banks to obtain an average wall temperature of the matrix)

T_b arithmetic average of T_1 and T_2

S heat-transfer surface area of the tubes

Heat-transfer correlation based on bulk temperature. - The correlation of the average heat-transfer coefficients in which the physical properties of the air are evaluated at the average bulk temperature is shown in figure 5(a) where the Nusselt number hD/k_b is plotted against Reynolds number $\frac{G_o D}{\mu_b F}$. Data for three wall temperature levels are included. It should be noted that the minimum mass flow per unit cross-sectional area divided by the free-flow factor G_o/F is the maximum mass flow per unit cross-sectional area based on the minimum free-flow area of the matrix. Included for comparison is the McAdams single-wire equation (ref. 1), and the Grimison equation (ref. 1) which is calculated for the matrix reported herein. The Grimison investigation was made down to a Reynolds number of 2000, and therefore the line

representing these data was extrapolated down to the Reynolds number range of the present investigation. In the McAdams single-wire equation and the Grimison equation, the fluid physical properties are evaluated at the film temperature; however, they are included for comparison. It is seen that all the data agree very well with the McAdams single-wire equation and fall below the Grimison line. No trend with wall-temperature level can be noted.

Heat-transfer correlation based on film temperature. - To make the heat-transfer data compatible with the McAdams and Grimison equations, data were computed with the air properties evaluated at the average film temperature. Figure 5(b) shows a plot of Nusselt number hD/k_f plotted against Reynolds number G_oD/μ_fF. It is seen that there is some scatter in the data, with the data falling progressively lower as the wall temperature is increased. The data fall approximately 10 percent below the McAdams single-wire line and have about the same slope. The data fall about 33 percent low when compared with the Grimison equation.

The transient wire-screen heat-transfer data of Coppage reported in reference 2 show that the heat-transfer data fall far below the McAdams single-wire correlation line at low free-flow factors and approach it as the free-flow factor is increased. At free-flow factors of 0.455 to 0.626, the heat-transfer data of Coppage fall approximately on the McAdams single-wire line. The data of the present investigation were obtained at a free-flow factor of 0.494 and are consistent with Coppage's results in that the data fall just 10 percent below the McAdams single-wire correlation line.

This would indicate that at relatively high free-flow factors, wires in any particular configuration act as single wires so far as heat transfer is concerned in that they are not greatly affected by the surrounding wires. At low free-flow factors, however, the heat-transfer characteristics of the wires are influenced by the other wires in close proximity with them.

Film heat-transfer correlation on porosity basis. - In reference 2 the transient wire-screen heat-transfer data of Coppage are correlated by plotting the Nusselt number hD/k_f against Reynolds number G_oD/μ_fP. It should be noted that the Reynolds number was modified by replacing the free-flow factor F with the porosity P. When the data of reference 2 were plotted in this manner, all the data, representing a range of free-flow factors from 0.156 to 0.626, fell on a single line represented by the equation

$$\frac{hD}{k_f} = 0.54\left(\frac{G_oD}{\mu_fP}\right)^{0.554}$$

The data of Coppage shown in reference 2 were obtained with wire screens, and a correction factor was applied to the equation just given to account for the heat-transfer area covered by the overlap of the wires. For the data of the present report, however, there is no correction since the matrix is made of parallel tubes with no cross wires and therefore no overlap.

Figure 5(c) shows a plot of Nusselt number hD/k_f against Reynolds number G_oD/μ_fP. As indicated, the physical properties of the air are evaluated at the average film temperature. Included for comparison is the correlation equation of reference 2. The data fall approximately 20 percent below the correlation equation of reference 2. There is some scatter in the data, the Nusselt number decreasing as the wall temperature is increased for a constant Reynolds number.

Bulk heat-transfer correlation on a porosity basis. - A plot of Nusselt number hD/k_b against Reynolds number G_oD/μ_bP is shown in figure 5(d). The physical properties of the air are evaluated at the average bulk temperature, and the Reynolds number is calculated on a porosity basis. It is seen that the data for the three wall temperatures fall on a single curve. Included for comparison is the line from reference 2 representing the heat-transfer data of Coppage. Comparison with this line is considered justified in that the data of Coppage were taken at very low heat-flux and temperature levels, and the data would not be noticeably altered by evaluating the physical properties on a different basis. The data of this investigation fall approximately 15 percent below the line of reference 2.

Modified heat-transfer correlation. - As shown by figure 5(a) there is no trend in the heat-transfer data with wall temperature level. However, if the wall temperature range were increased, a trend would be expected to appear, similar to that obtained in previous work on the flow of air through heated tubes. In the air heat-transfer investigation for flow through tubes as reported in reference 3, a trend with temperature was found, and a suitable correlation was reported by modifying the Reynolds number. A similar trend was found in the analytical and experimental investigation of reference 4. The Reynolds number was modified by substituting the product of the density at the film temperature and the bulk free-stream velocity for the conventional mass flow per unit cross-sectional area. This method was applied to the data of the present investigation by modifying the Reynolds number in the following manner

$$\frac{\rho_f V_b D}{\mu_f P} = \frac{G_o D}{\mu_f P}\frac{\rho_f}{\rho_b} = \frac{G_o D}{\mu_f P}\frac{T_b}{T_f}$$

A plot of Nusselt number hD/k_f against modified Reynolds number based on porosity $\rho_f V_b D/\mu_f P$ is shown in figure 6(a). It is seen that all the data fall on a single line and give results similar to the bulk heat-transfer correlation on a porosity basis. The data again fall approximately 15 percent below the line of reference 2 representing the data of Coppage.

Similar results were obtained when the Reynolds number based on free-flow factor was modified. A plot of Nusselt number hD/k_f against the modified Reynolds number based on free-flow factor $\rho_f V_b D/\mu_f F$ is shown in figure 6(b). The data fall within 10 percent of a line representing the McAdams single-wire equation.

Until further experimental work has been done, no statement can be made as to whether free-flow factor or porosity correlates the wire matrix data. Different configurations with various porosities and higher wall temperatures must be investigated before any definite conclusion can be obtained.

Correlation of Pressure-Drop Data

Wire-screen pressure-drop data of various investigators. - An extensive literature survey showed that a considerable amount of isothermal wire-screen pressure-drop data was available for comparison; however, no data were found for flow with heat transfer. The isothermal data from these various sources covered a wide range of variables including: Reynolds number, mesh size, free-flow factor, porosity, wire size, and number of banks. It should be noted that the matrix of the present investigation differs from those of the other investigations in that it has no cross wires.

The drag coefficient $\Delta p/qN$ was plotted against Reynolds number $G_O D/\mu_b F$ for the wire-screen data. It was found that at Reynolds numbers of about 300 and above, the coefficient $\Delta p/qN$ was generally independent of Reynolds number and increased with decreasing free-flow factor. All the basic data were not included in many of the references, and some assumptions were necessarily made in order to reduce the data to a usable form. The pressure drop Δp, with the exception of reference 5, was taken as the measured pressure drop across the screen with no corrections. The velocity head q was based on the frontal area of the screen and the upstream density. The pressure-drop data of reference 5 were corrected for momentum pressure-drop loss, and the density was taken as the average density in the wire screen matrix. The data of reference 5 were modified inasmuch as the Reynolds number range is high, and the density change through the test section becomes important.

Inasmuch as for the higher range of Reynolds numbers the drag coefficient $\Delta p/qN$ is independent of Reynolds number, a plot of $\Delta p/qN$ against free-flow factor F is shown in figure 7. Data from references 5 to 9 are included, as well as a data point from the present investigation. The best line through the data can be represented by the equation

$$\frac{\Delta p}{qN} = 0.215\ F^{-2.69}$$

the dotted line was taken from reference 2 and represents the wire-screen data of that report. The equation representing the dotted line is

$$\frac{\Delta p'}{q'N} = 0.38\ F^{-2.3}$$

It is interesting to note that the data of the present report fall on the dotted line of reference 2.

Correlation of pressure-drop data of the present investigation. - The modified drag coefficient was determined from figure 7 and is defined as follows:

$$C_D' = \frac{\Delta p'}{qN} F^{2.69}$$

The equation with the free-flow factor raised to the 2.69 power was chosen, since most of the data of the various references fall on this line. Figure 8 shows a plot of the modified drag coefficient C_D' against Reynolds number G_0D/μ_bF for the data of the present investigation. Data for three wall temperature levels as well as the isothermal case are included. The physical properties of the air are based on the average bulk temperature. The velocity head q' is based on the frontal area of the matrix and the average of the inlet and outlet air density. The pressure drop $\Delta p'$ is defined as follows:

$$\Delta p' = \Delta p - \Delta p_{en} - \Delta p_{mom} - \Delta p_{ex}$$

where:

Δp measured static-pressure drop across tube matrix

Δp_{en} entrance pressure loss

Δp_{mom} momentum pressure loss

Δp_{ex} exit pressure regain

It should be noted that the entrance pressure loss Δp_{en} and the exit pressure regain Δp_{ex} are opposite in sign and nearly equal in magnitude; therefore, the net result of these two corrections is insignificant. The various terms were computed with the aid of the following schematic diagram of the test section showing the different stations:

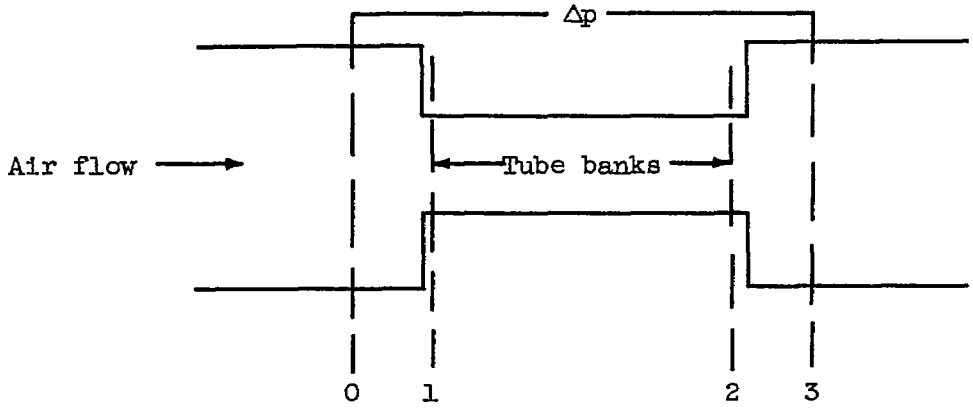

$$\Delta p_{en} = p_0 - p_1 = \frac{G_1^2}{2g\rho_b}(1 - F)^2$$

$$\Delta p_{ex} = p_2 - p_3 = \frac{G_0^2}{g\rho_0}\left(\frac{1 + \Delta t/t_0}{1 - \Delta p/p_0}\right)\left(1 - \frac{1}{F}\right)$$

The equations are calculated assuming incompressible flow and are derived in reference 10. The static temperature t was assumed to be equal to the total temperature T; for the range of flow and heat flux encountered in this investigation, this assumption was found to be valid. When sample calculations were made to determine the entrance loss and exit regain with compressible-flow equations, no significant difference was noted for the range of temperatures and flows of the present investigation.

The momentum pressure loss was determined as follows:

$$\Delta p_{mom} = \frac{G_1^2}{g}\left(\frac{1}{\rho_2} - \frac{1}{\rho_1}\right)$$

It is seen that in the low Reynolds number range, the drag coefficients decrease as the Reynolds number is increased. The coefficients become almost independent of Reynolds number above a Reynolds number of about 400. The data hold together fairly well, and no definite trend with wall temperature level exists for the temperature range investigated.

It should be noted that no measurable static-pressure difference existed among the three entrance static taps or among the three exit static taps.

Comparison of data. - The pressure-drop data of the present investigation are shown in figure 9 where $\Delta p'/q'$ is plotted against the Reynolds number $G_O D/\mu_b F$. Included for comparison is the following equation from reference 11:

$$\frac{\Delta p'}{q'} = \frac{0.38}{F^{2.3}} N^{0.98}$$

A correction factor for $\Delta p'/q'$ is given in reference 11. This correction factor varies from 1 at a Reynolds number of 1000 to 1.2 at a Reynolds number of 200. This correction factor was not applied, as the data of the present investigation check the predicted line very well at Reynolds numbers of about 500 and above. No explanation for this difference can be given at this time.

SUMMARY OF RESULTS

An experimental investigation of forced-convection heat-transfer and pressure-drop characteristics of a closely spaced electrically heated wire matrix over a range of Reynolds numbers (based on wire diameter and maximum velocity) from 82 to 1900, average wire temperatures up to 1109° R, and heat flux densities up to 84,000 Btu per hour per square foot gave the following results:

1. The wire-matrix heat-transfer data evaluating the properties of air at film temperature agreed fairly well with the McAdams single-wire equation, but fell below the equation for Grimison's tube bank data.

2. When the data were modified by basing the Reynolds number on the porosity, the data fell slightly low when compared with the line recommended by Jordan and Lapides. A further modification of the Reynolds number, in which the product of the density at the film temperature and the bulk upstream velocity was substituted for the conventional mass flow per unit cross-sectional area, resulted in a good correlation of the data; the correlation was slightly low when compared to a line

representing the data of Jordan and Lapides. However, until a range of configurations, porosities, and higher surface temperatures is investigated, the correlation can be considered only preliminary.

3. Drag coefficients for isothermal wire-screen pressure-drop data of various investigators were compared on a free-flow factor basis for Reynolds numbers above 300. The best line through this data can be represented by the equation $\Delta p/qN = 0.215\ F^{-2.69}$. This correlation was applied to pressure drop data with and without heat addition.

Lewis Flight Propulsion Laboratory
National Advisory Committee for Aeronautics
Cleveland, Ohio, April 15, 1954

APPENDIX - SYMBOLS

The following symbols are used in this report:

C_D	drag coefficient, $\Delta p/qN$
C_D'	modified drag coefficient, $\frac{\Delta p' F^{2.69}}{q'N}$
c_p	specific heat of air, Btu/(lb)(°F)
D	outside diameter of tube or wire in matrix, ft
F	free-flow factor of matrix
G	mass flow per unit cross-sectional area, lb/(hr)(sq ft)
g	acceleration due to gravity, $(4.17 \times 10^8$ ft/hr$^2)$
h	average heat-transfer coefficient, Btu/(hr)(sq ft)(°F)
k	thermal conductivity of air, Btu/(hr)(sq ft)(°F/ft)
N	number of tube or screen banks
P	porosity of matrix (volume of voids in matrix/total volume of matrix)
p	static pressure, lb/sq ft
Δp	over-all measured static-pressure drop across matrix, lb/(sq ft)
$\Delta p'$	corrected static-pressure drop across matrix, lb/sq ft
Δp_{en}	entrance pressure loss, lb/sq ft
Δp_{ex}	exit pressure regain, lb/sq ft
Δp_{mom}	momentum pressure drop, lb/sq ft
Q	rate of heat transfer to air, Btu/hr
q	velocity head, $G_o^2/2g\rho_o$, lb/sq ft

q'	modified velocity head, $G_0^2/2g\rho_{av}$, lb/sq ft
Q_P	rate of electrical power input to test section, Btu/hr
S	heat-transfer area of tubes in matrix, sq ft
T_b	average bulk temperature, $(T_1 + T_2)/2$, $^\circ R$
T_f	average film temperature, $(T_s + T_b)/2$, $^\circ R$
T_s	average surface temperature of matrix, $^\circ R$
T_w	average bank temperature, $^\circ R$
T_1	air temperature at entrance to tube matrix, $^\circ R$
T_2	air temperature at exit of tube matrix, $^\circ R$
t	static temperature, $^\circ R$
Δt	static temperature difference from inlet to outlet of matrix, $^\circ R$
V_b	upstream air velocity, ft/hr
W	air flow, lb/hr
μ	absolute viscosity of air, lb/(hr)(ft)
ρ	density of air, lb/ft^3
$\frac{G_0 D}{\mu F}$	Reynolds number based on free-flow factor
$\frac{G_0 D}{\mu P}$	Reynolds number based on porosity
$\frac{\rho_f V_b D}{\mu_f F}$	modified Reynolds number based on free-flow factor
$\frac{\rho_f V_b D}{\mu_f P}$	modified Reynolds number based on porosity
$\frac{hD}{k}$	Nusselt number

Subscripts:

av	average
b	bulk (when applied to properties, indicates evaluation at average bulk properties, T_b)
f	film (when applied to properties, indicates evaluation at average film temperature, T_f)
0	station before matrix entrance
1	test section entrance
2	test section exit
3	station after matrix exit

REFERENCES

1. McAdams, William H.: Heat Transmission. Second ed., McGraw-Hill Book Co., Inc., 1942.

2. Lapides, M. E., and Lawyer, J. E.: Summary of Analysis of Heat Transfer & Pressure Drop Information & Estimates Applicable to AC-1 Fuel Elements. DC 53-3-10, General Electric Dev., ANP Proj., Feb. 5, 1953.

3. Humble, Leroy V., Lowdermilk, Warren H., and Desmon, Leland G.: Measurements of Average Heat-Transfer and Friction Coefficients for Subsonic Flow of Air in Smooth Tubes at High Surface and Fluid Temperatures. NACA Rep. 1020, 1951. (Supersedes NACA RM's E7L31, E8L03, E50E23, and E50H23.)

4. Deissler, R. G., and Eian, C. S.: Analytical and Experimental Investigation of Fully Developed Turbulent Flow of Air in a Smooth Tube with Heat Transfer with Variable Fluid Properties. NACA TN 2629, 1952.

5. Adler, Alfred A.: Variation with Mach Number of Static and Total Pressures Through Various Screens. NACA WR L-23, 1946. (Supersedes NACA CB L5F28.)

6. Eckert, B., and Pflüger, F.: The Resistance Coefficient of Commercial Round Wire Grids. NACA TM 1003, 1942.

7. Schubauer, G. B., Spangenberg, W. G., and Klebanoff, P. S.: Aerodynamic Characteristics of Damping Screens. NACA TN 2001, 1950.

8. Jordan, L., and Lapides, M.: Initial Experimental Investigation of Pressure Drop for Flow Normal to Series of Screens. DC-52-32-72, General Electric Dev., ANP Proj., Task 7313, Dec. 12, 1952.

9. McDonough, Robert: Air Flow Tests of Regenerative Heat Exchanger Sections. Rep. No. RER-118, Harrison Radiator Div., General Motors Corp., July 15, 1948.

10. Sams, Eldon W., and Nagey, Tibor F.: Measurements of Pressure Drop with no Heat Addition on Mockup Segments of the General Electric Air-Cooled Aircraft Reactor. NACA RM E52I05, 1952.

11. Jordan, L. D., and Lapides, M. E.: Experimental Investigation of Pressure Drop for Flow Normal to Series of Screens. DC 53-3-84, General Electric Dev., ANP Proj., Mar. 12, 1953.

TABLE I. - BASIC EXPERIMENTAL ISOTHERMAL DATA

Run	T_o, °R	W, lb/hr	G_o, lb/(hr)(sq ft)	$\frac{G_o D}{\mu_f F}$	Δp, lb/sq ft	Δp_{mom}, lb/sq ft	$\Delta p'$, lb/sq ft	ρ_{av}, lb/cu ft	q', lb/sq ft	C_D'
1	543	36.1	1,368	103	0.80	(1)	0.77	0.0713	0.031	0.455
2	542	40.6	1,539	116	1.02	(1)	.98	.0715	.040	.458
3	542	45.9	1,739	131	1.23	(1)	1.18	.0715	.051	.433
4	543	52.8	1,999	150	1.56	(1)	1.49	.0713	.067	.413
5	542	62.3	2,361	178	2.01	(1)	1.91	.0715	.094	.381
6	544	88.4	3,350	251	3.60	(1)	3.39	.0712	.189	.334
7	544	112.4	4,256	319	5.51	0.01	5.18	.0713	.305	.316
8	544	129.6	4,909	369	7.09	.01	6.64	.0713	.405	.305
9	544	143.4	5,431	408	8.54	.02	8.00	.0713	.496	.300
10	544	156.0	5,908	443	9.97	.02	9.32	.0713	.587	.296
11	544	221.7	8,398	630	20.72	.09	19.39	.0714	1.184	.305
12	544	276.5	10,466	786	29.76	.20	27.65	.0715	1.836	.280
13	536	165.0	6,249	474	10.64	.03	9.93	.0728	.644	.288
14	536	193.2	7,319	556	14.17	.05	13.19	.0728	.882	.279
15	536	224.7	8,511	646	19.93	.09	18.59	.0729	1.192	.291
16	536	258.2	9,780	742	24.50	.14	22.71	.0729	1.573	.269
17	536	291.2	10,828	837	30.69	.23	28.25	.0730	1.926	.263
18	536	305.9	11,587	880	34.91	.28	32.35	.0731	2.204	.274
19	539	335.4	12,704	962	45.47	.32	42.44	.0730	2.651	.298
20	540	370.9	14,051	1063	57.28	.49	53.26	.0731	3.239	.306
21	536	438.1	16,595	1260	74.77	1.24	68.87	.0736	4.490	.286
22	540	497.6	18,849	1424	99.72	2.04	92.16	.0734	5.805	.296
23	539	530.5	20,093	1518	106.46	2.58	97.68	.0735	6.586	.276
24	546	592.9	22,459	1688	151.44	3.71	140.13	.0737	8.211	.318
25	542	658.9	24,958	1882	184.22	6.33	169.07	.0743	10.047	.313
26	534	116.4	4,411	336	5.45	(1)	5.12	.0741	.315	.304
27	534	191.2	7,242	552	13.49	(1)	12.60	.0742	.847	.277
28	534	238.9	9,048	690	21.31	.02	19.90	.0743	1.321	.281
29	534	278.4	10,548	804	27.61	.07	25.67	.0744	1.793	.267
30	534	114.6	4,342	331	5.24	(1)	4.92	.0741	.305	.301
31	534	188.4	7,137	544	13.12	(1)	12.26	.0742	.823	.278
32	534	242.8	9,196	701	22.26	.03	20.80	.0743	1.364	.284
33	534	284.4	10,771	821	28.76	.08	26.72	.0744	1.870	.266

[1] Δp_{mom} was less than 0.01 lb/sq ft.

TABLE II. - BASIC EXPERIMENTAL HEAT-TRANSFER DATA

Run	T_0, °R	$T_3 - T_0$, °F	T_s, °R	W, lb/hr	G_0, lb/(hr)(sq ft)	Q, Btu/hr	Q/S, Btu/(hr)(sq ft)	h, Btu/(hr)(sq ft)(°F)	$\frac{hD}{k_b}$	$\frac{hD}{k_f}$	$\frac{G_0D}{\mu_f F}$	$\frac{G_0D}{\mu_f F}$	Δp, lb/sq ft	$\Delta p'$, lb/sq ft	ρ_{av}, lb/cu ft	q', lb/sq ft	C_D'
34	548	131	690	42.7	1,819	1,343	4,009	52.6	5.1	4.9	111	109	0.09	1.20	0.0642	0.049	0.456
35	547	118	689	57.7	2,185	1,630	4,867	60.1	5.9	5.6	132	145	.14	1.89	.0649	.088	.399
36	547	103	684	79.9	2,950	1,925	5,747	67.0	6.7	6.3	208	196	.23	3.08	.0656	.159	.361
37	547	101	694	104.4	3,955	2,541	7,584	77.9	7.8	7.3	278	258	.48	5.20	.0658	.285	.340
38	537	97	695	147.9	5,601	3,459	10,326	94.4	9.6	8.8	398	373	.80	9.70	.0672	.554	.323
39	537	84	686	181.6	6,880	3,676	10,974	102.8	10.5	9.7	493	462	1.06	13.53	.0679	.835	.302
40	537	80	688	226.8	8,590	4,351	12,987	117.0	12.0	11.1	617	578	1.60	20.28	.0683	1.296	.291
41	538	71	685	303.6	11,500	5,175	15,449	137.2	14.4	13.3	830	775	2.69	33.40	.0688	2.308	.270
42	538	67	683	359.3	13,609	5,804	17,327	158.3	16.2	14.9	987	920	3.78	47.54	.0692	3.210	.276
43	540	64	685	429.2	16,259	6,554	18,563	172.4	17.9	16.4	1178	1094	5.51	66.85	.0694	4.567	.273
44	541	58	685	533.8	20,219	7,521	22,450	196.0	20.4	18.7	1467	1367	9.00	102.23	.0700	7.000	.272
45	544	54	687	610.8	23,136	7,932	23,678	204.0	21.2	19.4	1678	1565	12.49	138.27	.0704	9.112	.283
46	552	331	909	48.6	1,840	3,885	11,597	60.4	5.1	4.6	113	105	0.29	1.91	0.0575	0.071	0.504
47	553	317	919	63.4	2,401	4,857	14,499	69.9	6.0	5.3	148	135	.46	2.92	.0578	.120	.455
48	553	279	918	87.4	3,309	5,885	17,567	77.9	6.8	6.0	208	186	.78	4.86	.0588	.223	.405
49	552	249	941	136.3	5,163	8,179	24,416	92.2	8.3	7.1	330	291	1.70	10.29	.0599	.534	.359
50	549	333	980	89.1	3,375	7,175	21,418	81.1	6.9	6.0	207	184	.97	5.23	.0577	.257	.411
51	548	277	919	87.6	3,318	5,880	17,493	75.1	6.6	5.8	210	188	.78	4.80	.0592	.223	.401
52	548	202	898	195.4	7,326	9,398	28,054	112.8	10.4	9.0	485	425	2.83	17.88	.0618	1.041	.320
53	547	185	916	281.0	10,644	12,405	37,030	138.8	13.0	11.1	711	620	5.57	32.63	.0628	2.164	.281
54	546	161	892	355.0	13,447	13,732	40,991	154.6	14.8	12.5	910	792	8.10	49.65	.0640	3.388	.273
55	546	152	895	429.8	16,280	15,753	47,024	172.7	16.6	14.0	1107	960	11.74	72.28	.0648	4.908	.274
56	544	132	858	516.1	19,549	16,339	48,773	198.4	19.3	16.4	1351	1180	15.69	100.51	.0662	6.918	.271
57	544	119	847	610.9	23,140	17,427	52,021	213.9	21.2	18.0	1611	1410	21.92	148.01	.0675	9.512	.286
58	550	411	967	36.6	1,388	3,644	10,878	51.3	4.2	3.7	82	71	0.20	1.23	0.0556	0.041	0.552
59	551	395	992	52.2	1,978	4,993	14,904	61.2	5.0	4.4	118	106	.39	2.13	.0558	.084	.472
60	551	358	966	62.3	2,358	5,388	16,084	68.2	5.7	5.0	143	129	.51	2.75	.0567	.118	.435
61	551	329	979	86.4	3,274	6,876	20,525	77.8	6.6	5.7	201	179	.90	4.77	.0574	.224	.397
62	553	336	1049	127.6	4,835	10,378	30,979	94.4	8.0	6.7	295	256	2.02	9.97	.0572	.490	.379
63	550	322	1075	165.9	6,283	12,930	38,597	106.2	9.1	7.5	388	331	3.29	15.28	.0578	.818	.348
64	549	267	1064	264.3	10,013	17,031	50,839	134.7	12.0	9.7	637	537	7.09	32.93	.0597	2.013	.305
65	549	242	1060	380.3	13,647	21,039	62,803	161.2	14.6	11.7	880	735	12.35	54.27	.0608	3.672	.275
66	549	238	1024	434.2	16,447	24,892	74,304	178.4	16.1	12.8	1062	877	18.14	75.53	.0613	5.291	.266
67	549	224	1109	523.4	19,824	28,263	84,357	188.1	17.2	13.4	1291	1050	25.95	105.84	.0622	7.574	.280

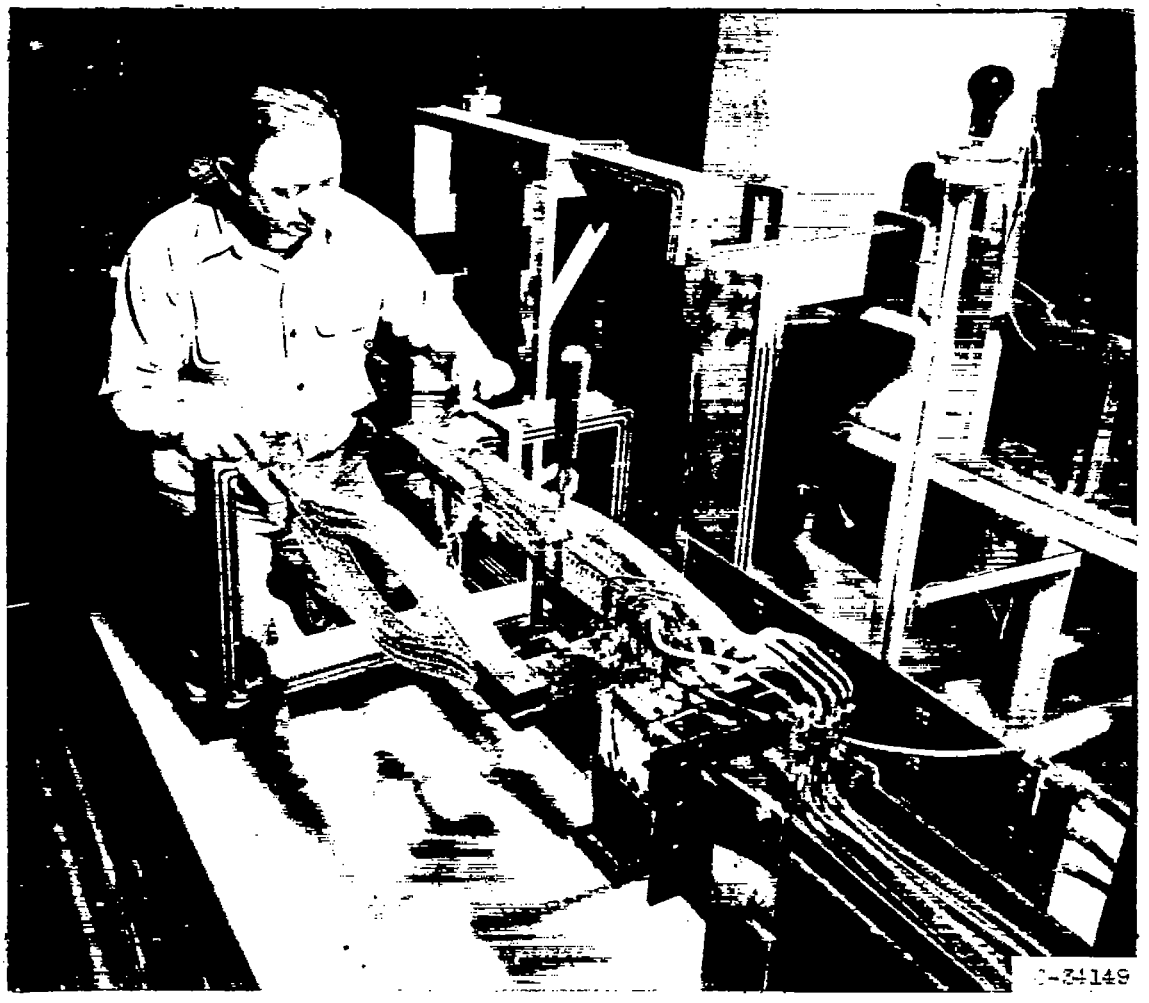

(a) Overall view.

Figure 1. · Test setup.

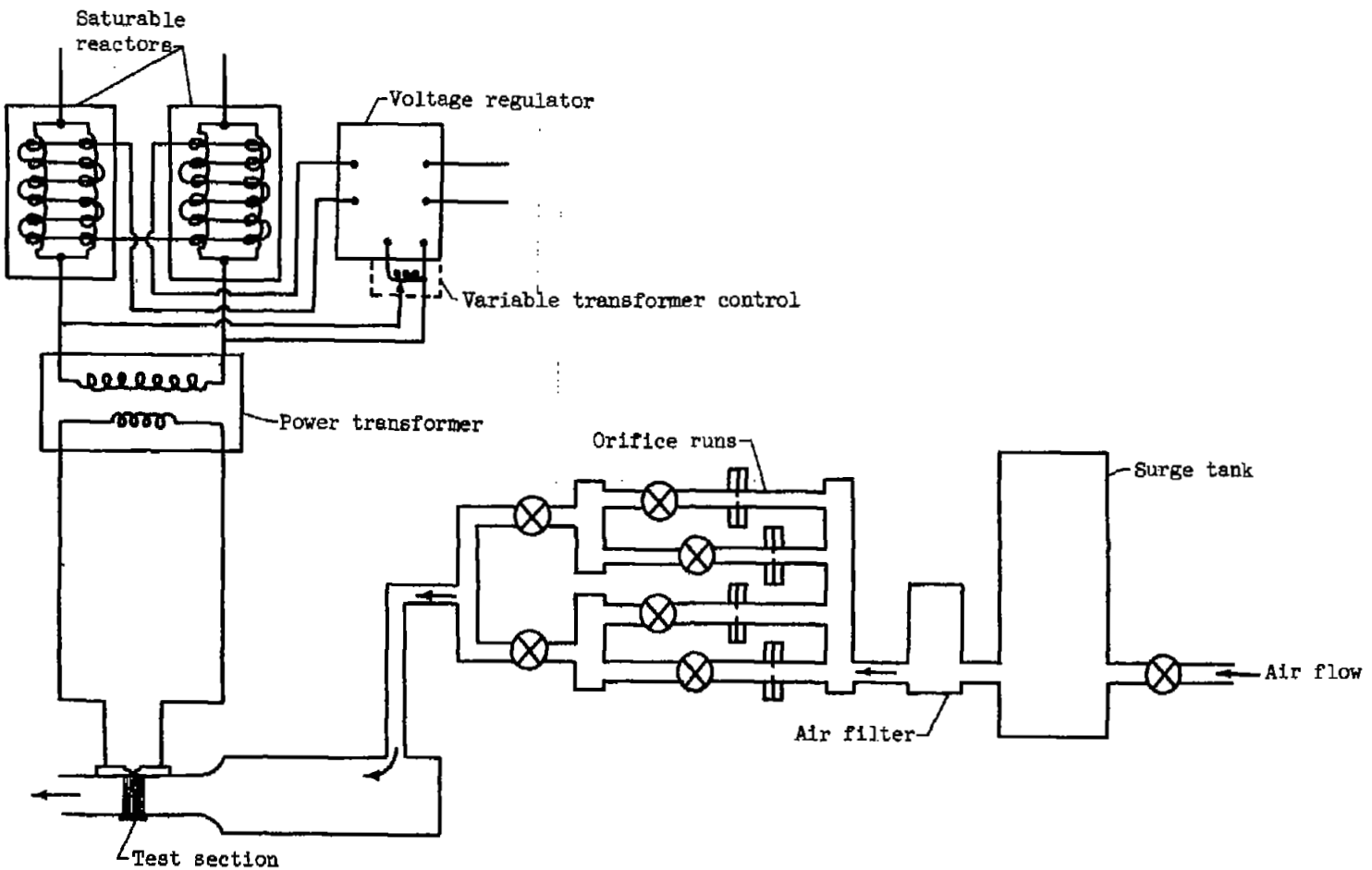

(b) Schematic drawing

Figure 1. - Concluded. Test setup.

3250

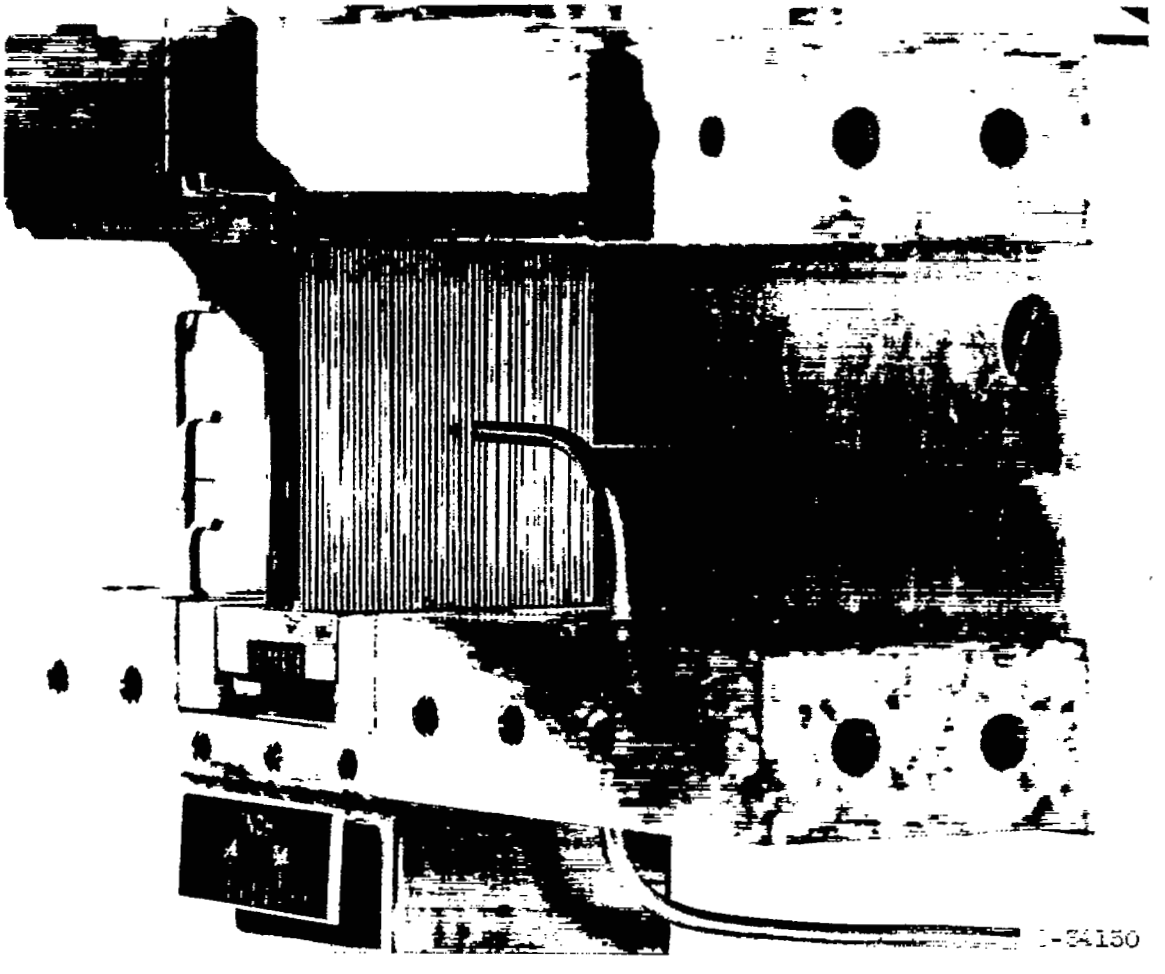

(a) Overall view.

Figure 2. - Test Section.

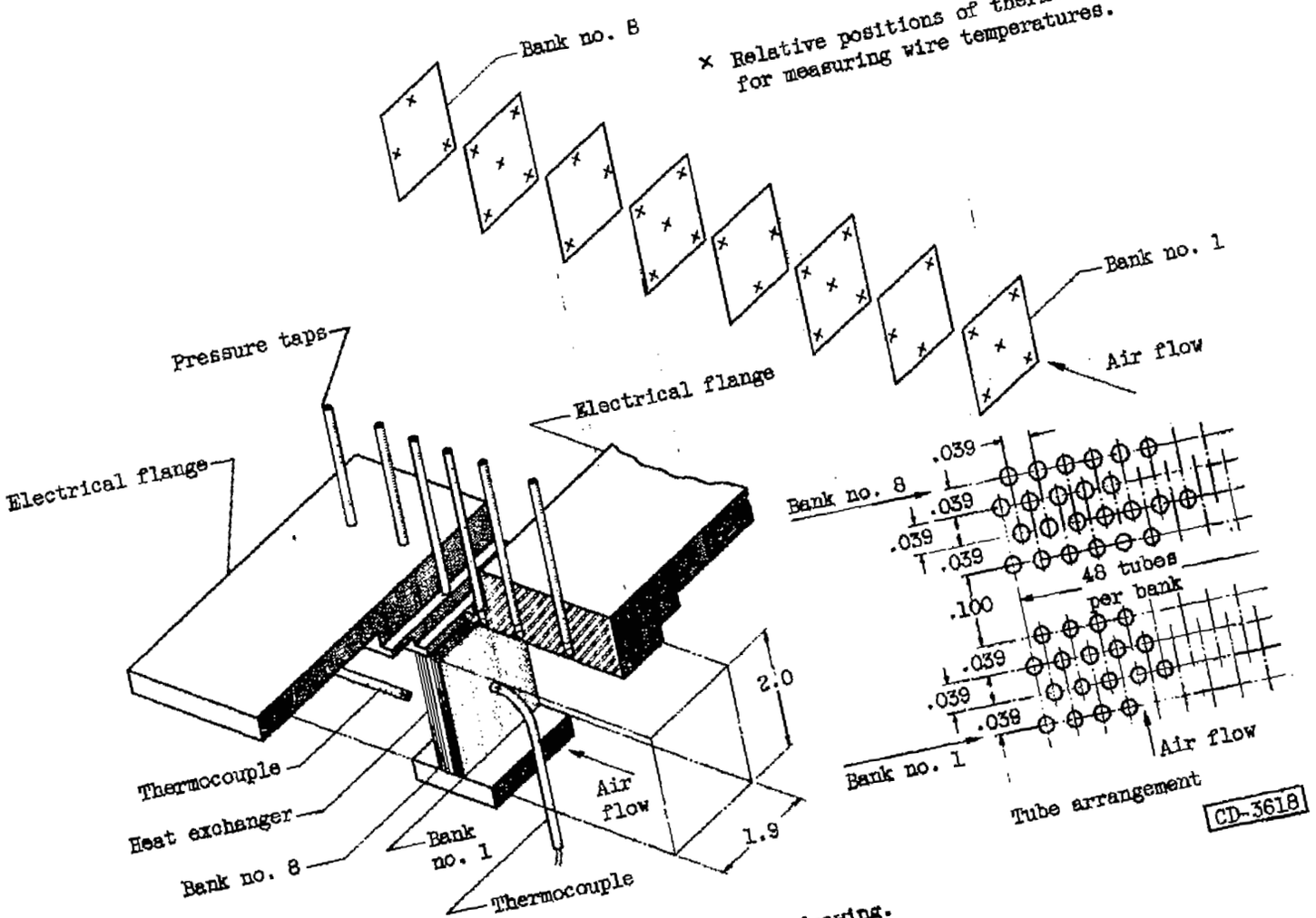

(b) Schematic drawing.

Figure 2. - Continued. Test section.

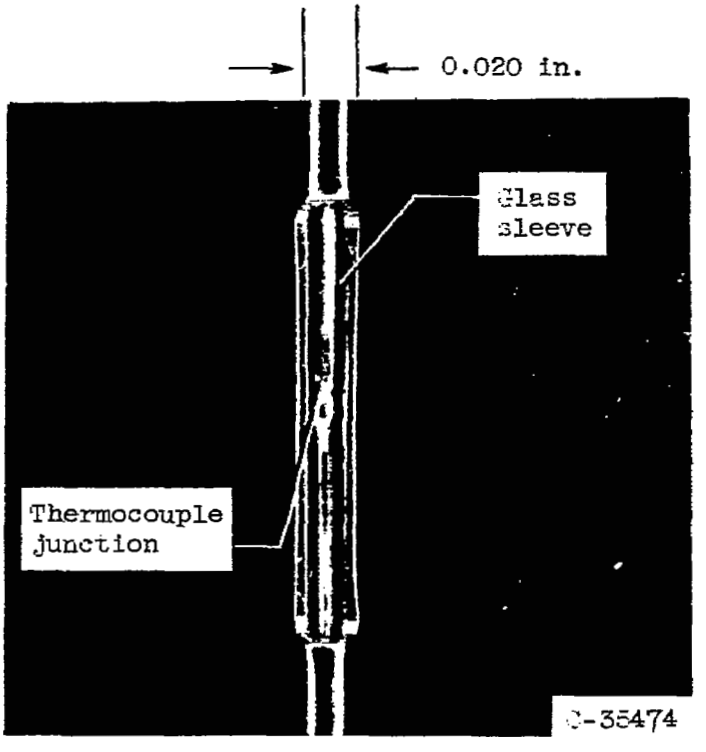

(c) Enlarged photograph of thermocouple installation in matrix element.

Figure 2. - Concluded. Test section.

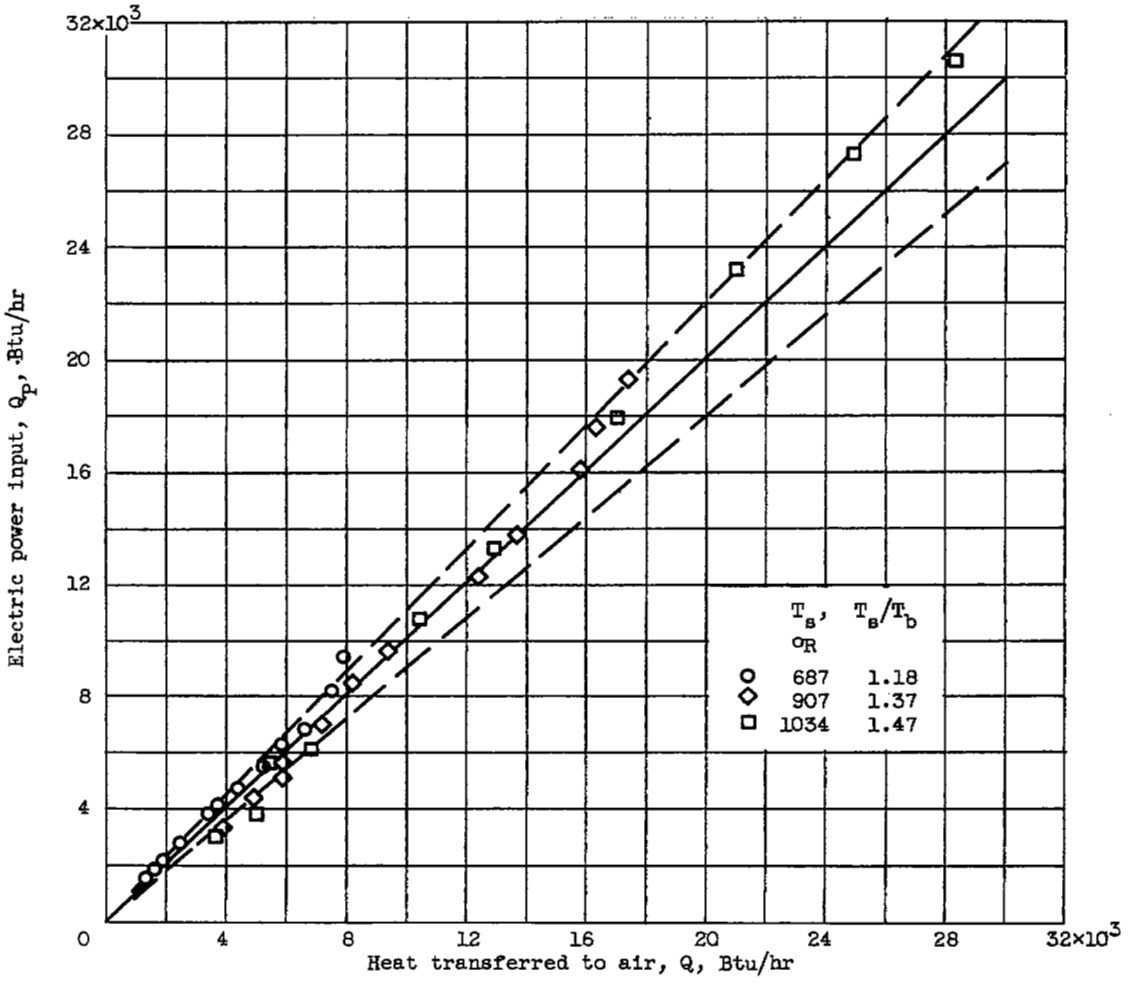

Figure 3. - Heat balance.

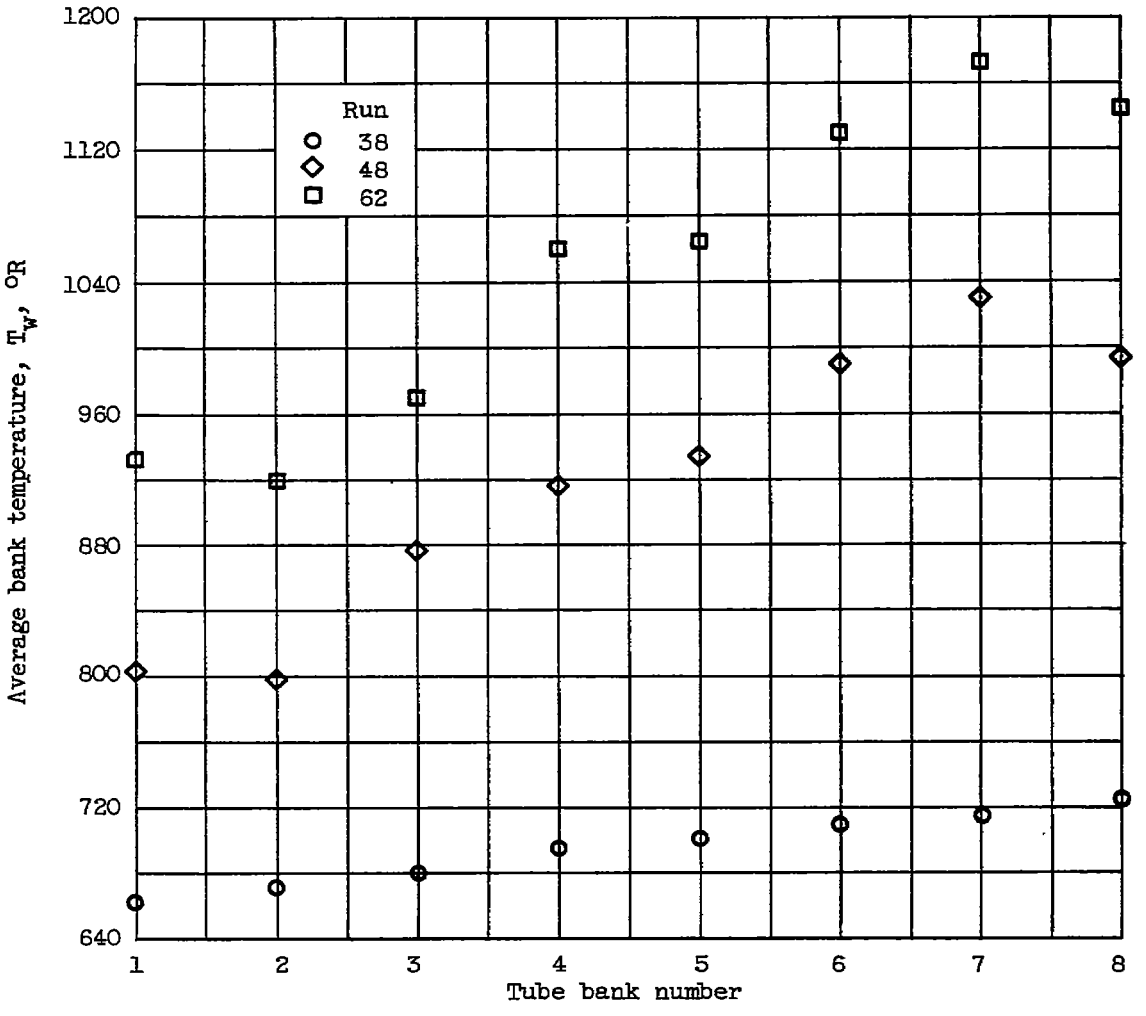

Figure 4. - Representative bank temperature distribution.

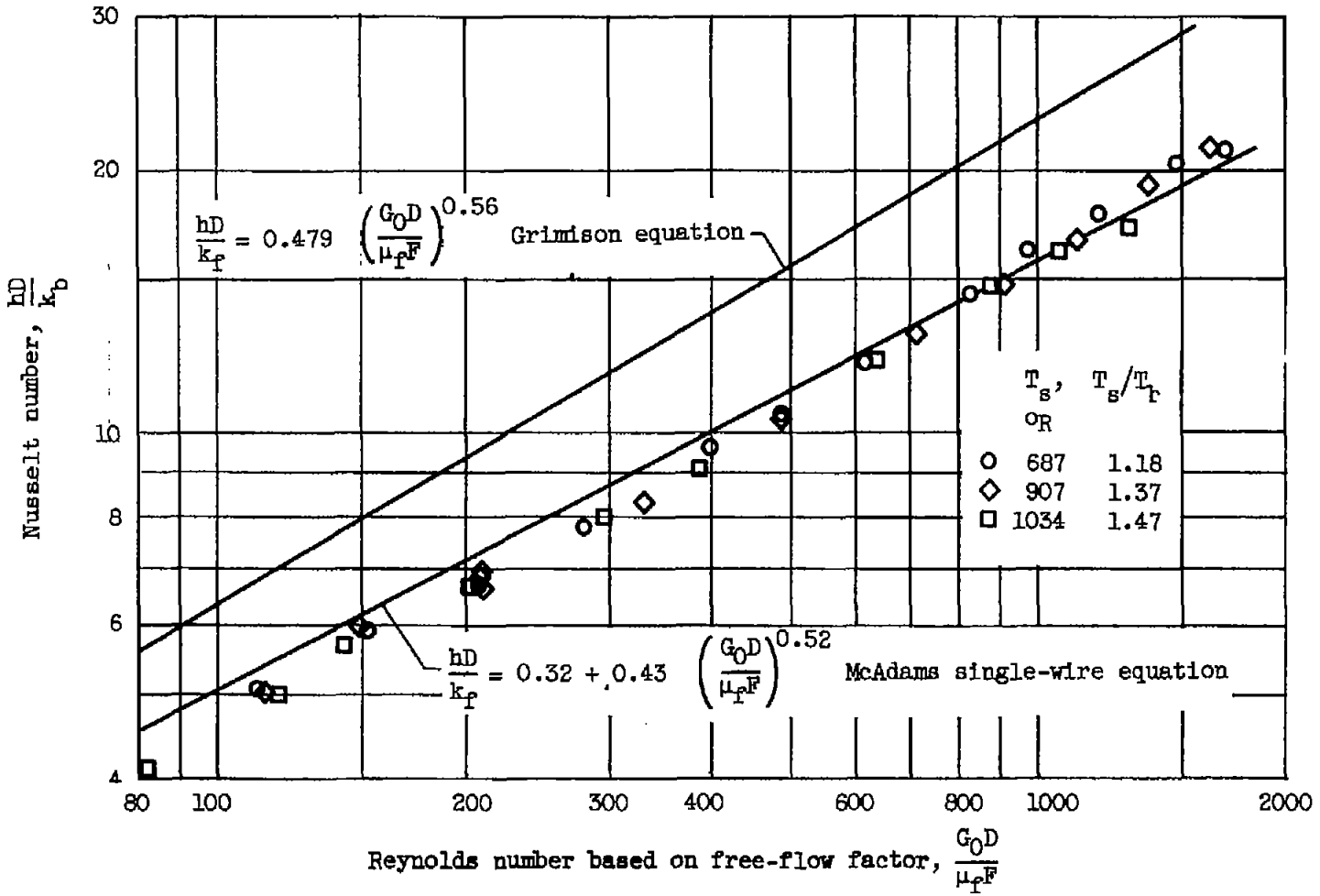

(a) Physical properties of air evaluated at average bulk temperature t_b.

Figure 5. - Heat-transfer correlation.

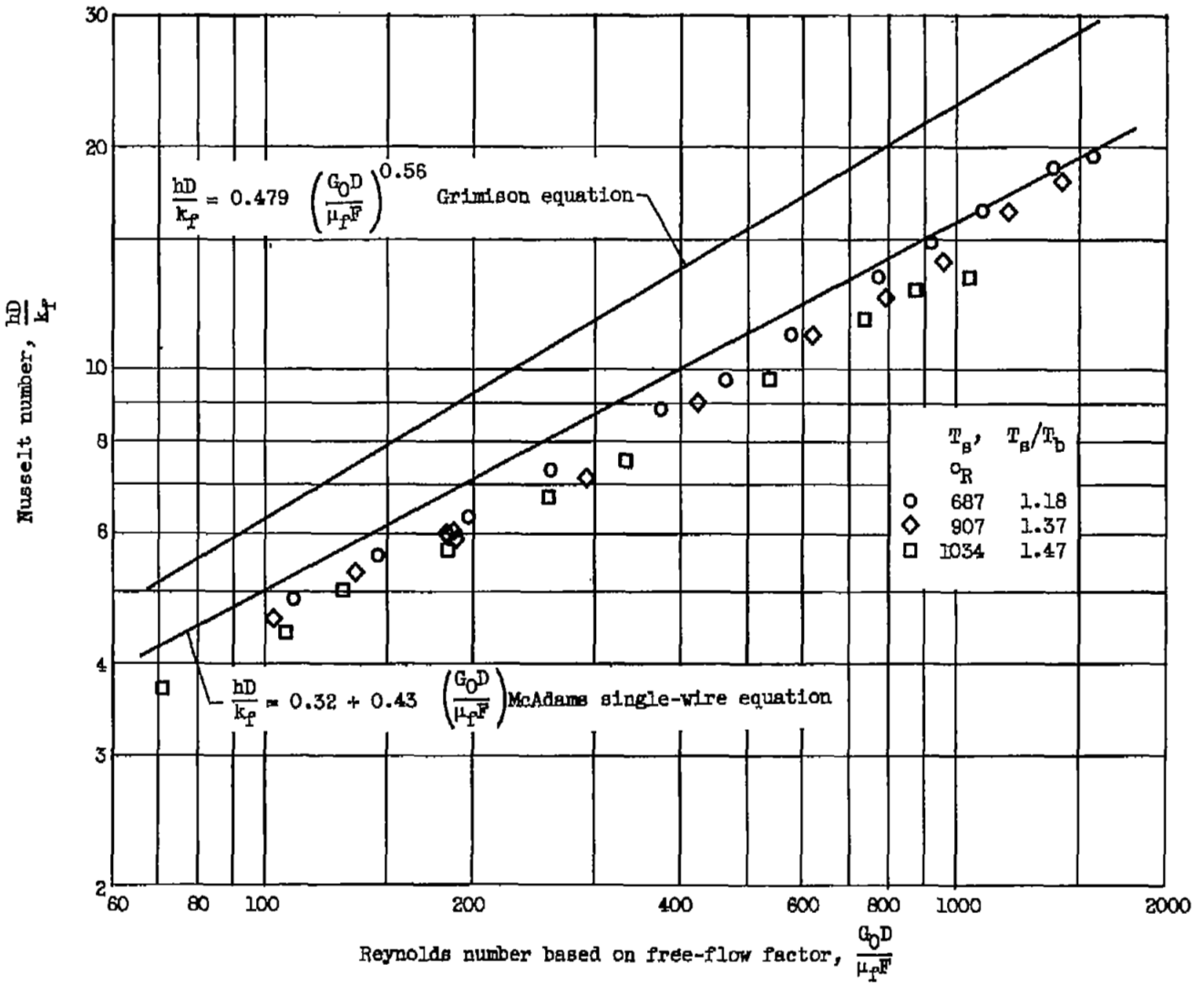

(b) Physical properties of air evaluated at average film temperature t_f.

Figure 5. - Continued. Heat-transfer correlation.

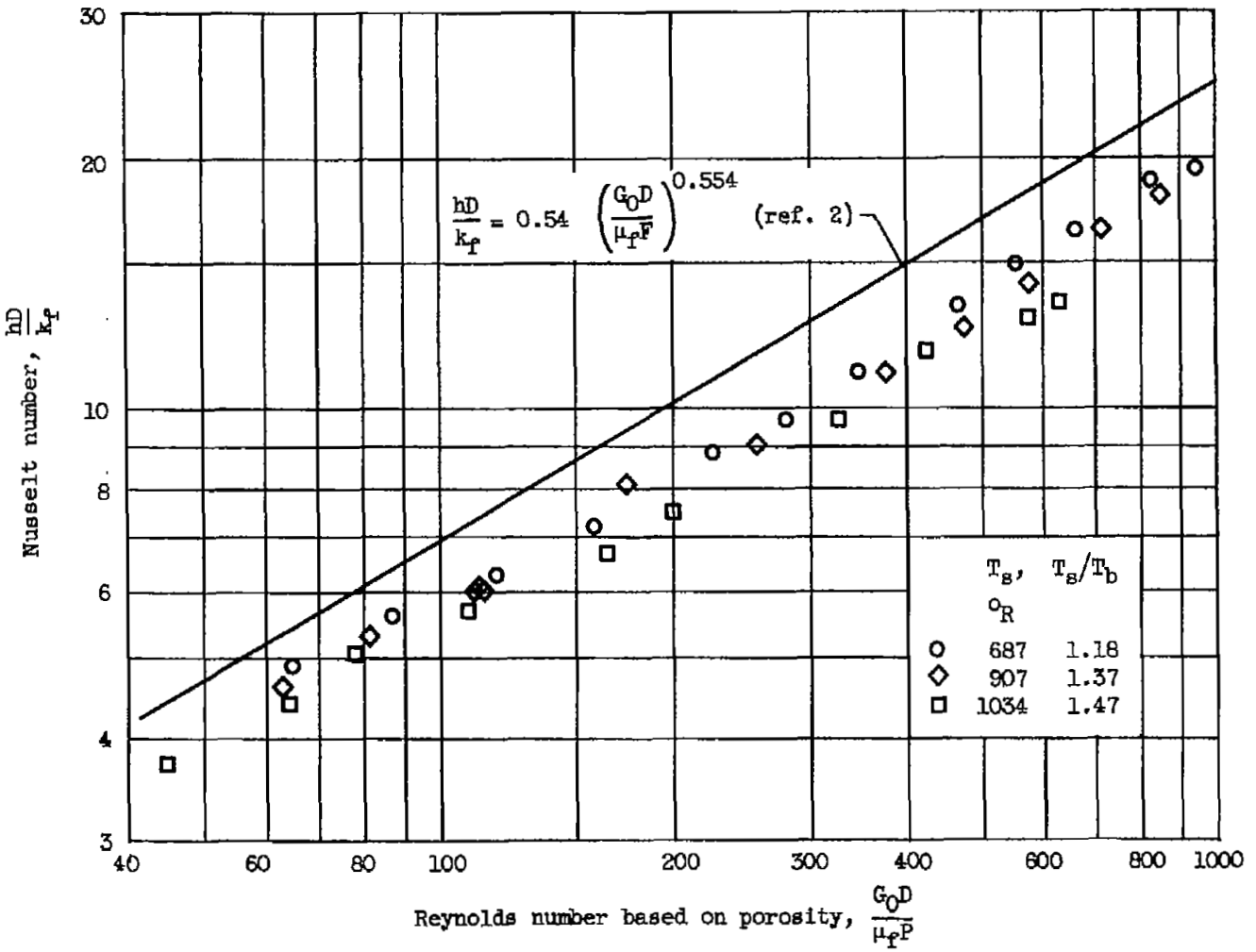

(c) Physical properties of air evaluated at average film temperature t_f; Reynolds number based on porosity P.

Figure 5. - Continued. Heat-transfer correlation.

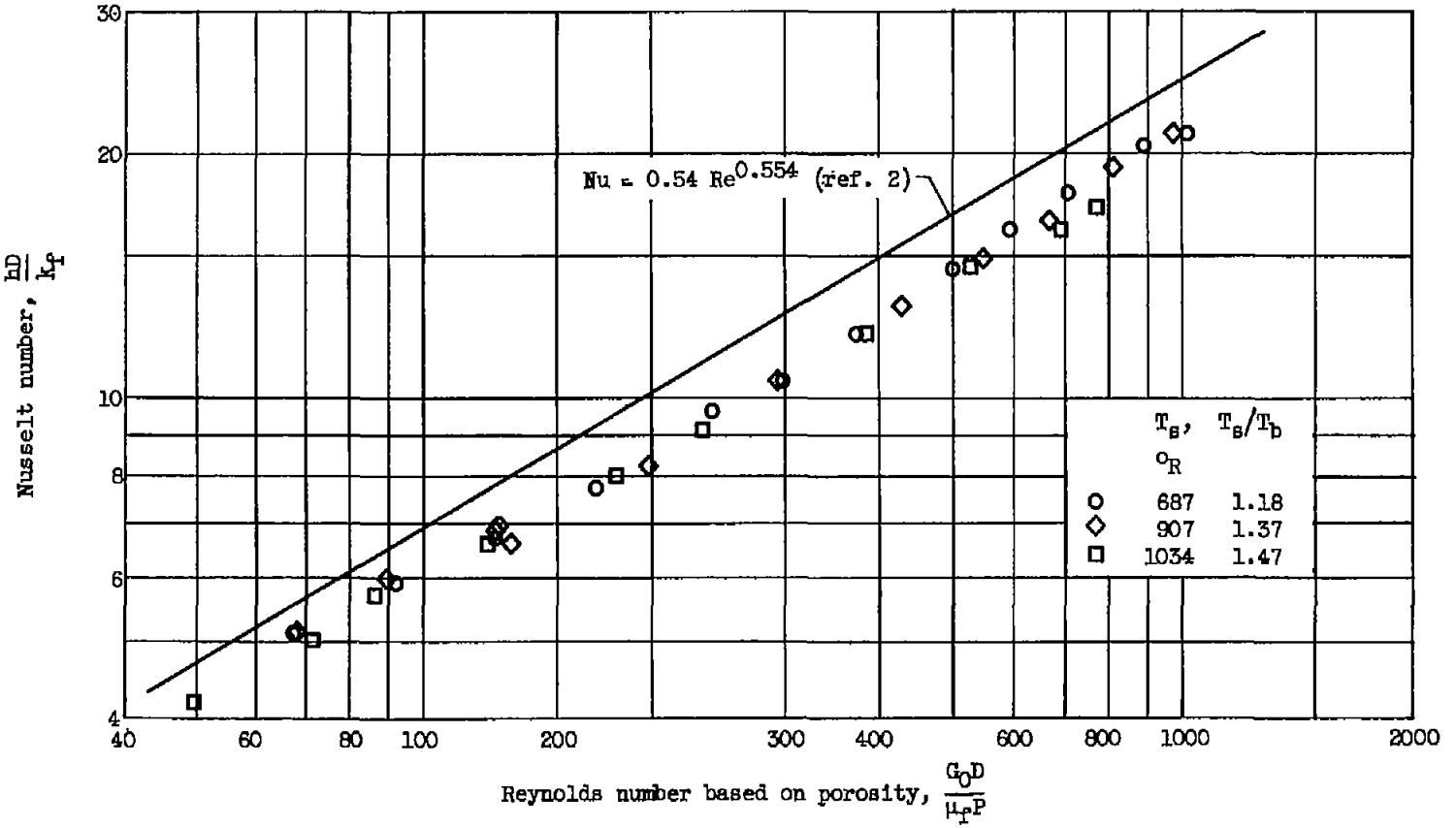

(d) Physical properties of air evaluated at average bulk temperature t_b; Reynolds number based on porosity P.

Figure 5. - Concluded. Heat-transfer correlation.

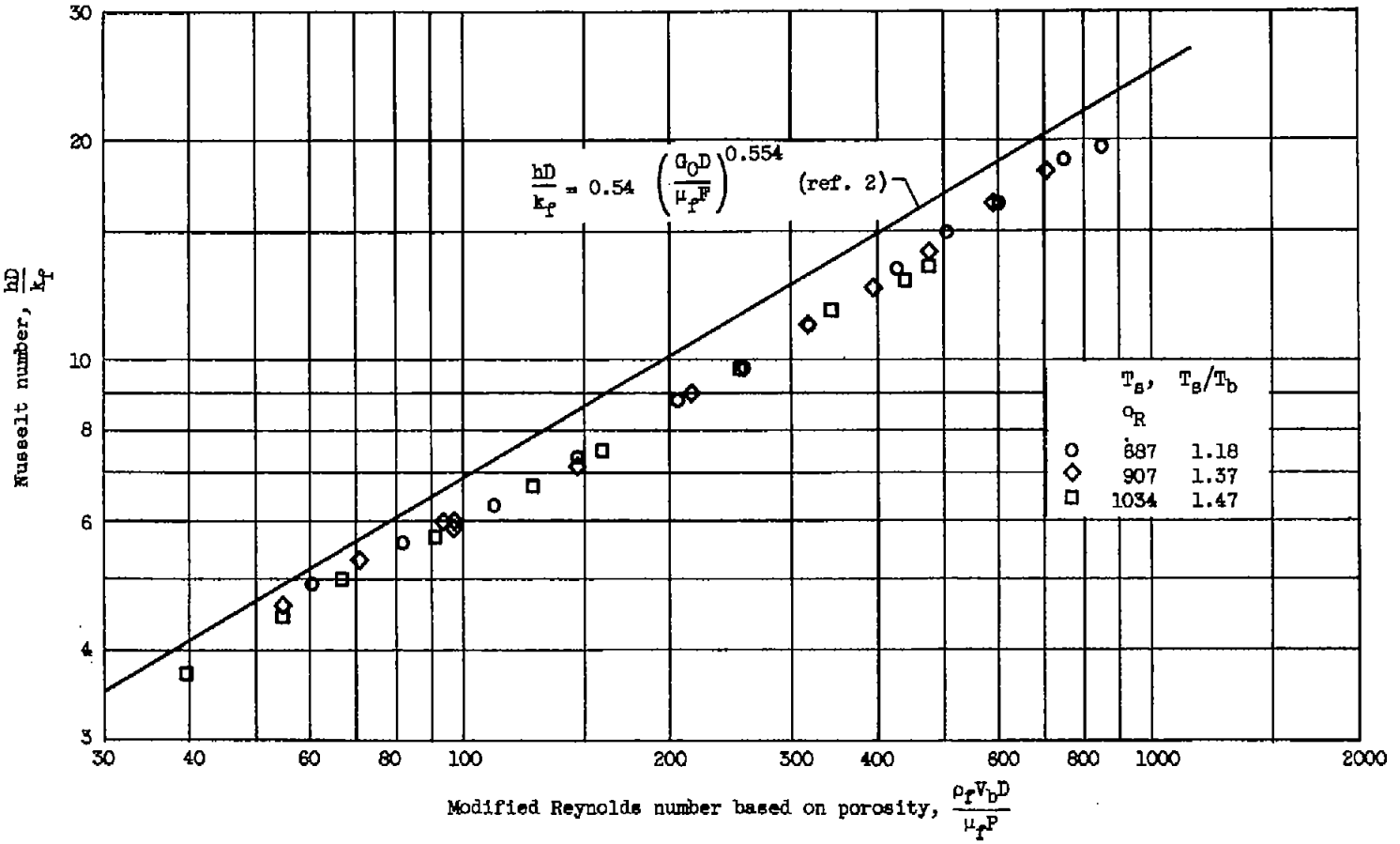

(a) Reynolds number based on porosity P.

Figure 6. - Modified heat-transfer correlation.

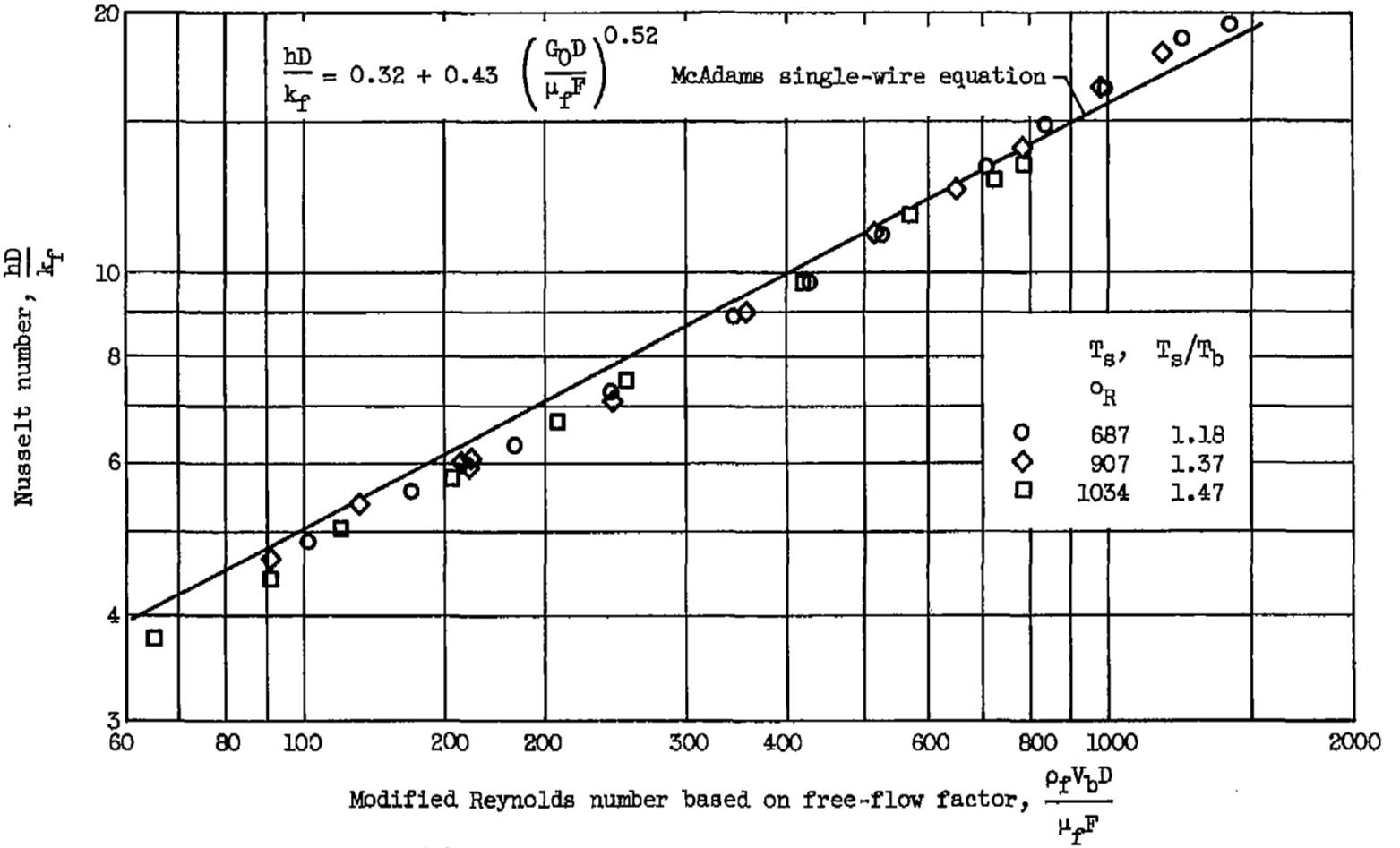

(b) Reynolds number based on free-flow factor F.

Figure 6. - Concluded. Modified heat-transfer correlation.

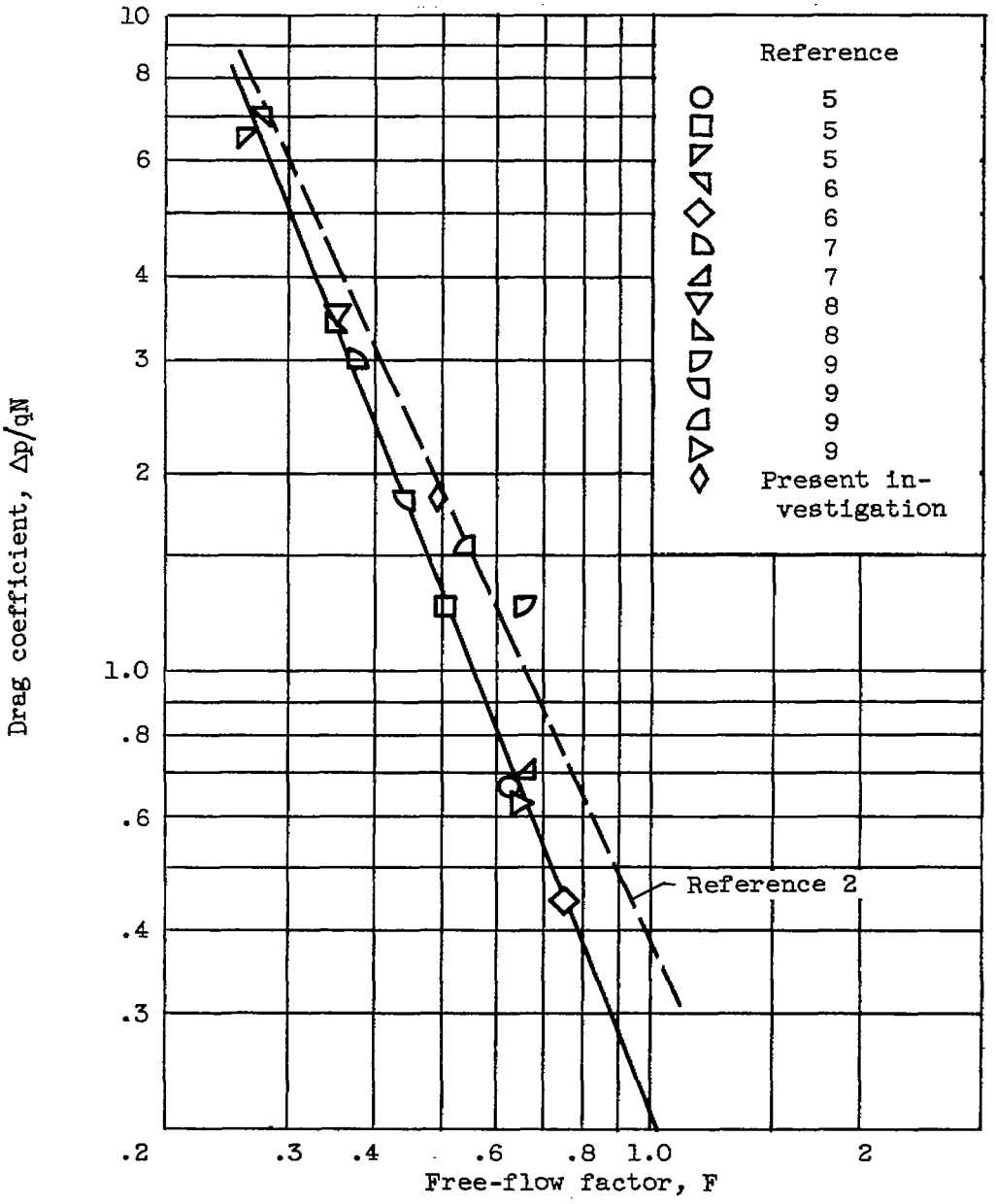

Figure 7. - Cross-plot of drag coefficient $\Delta p/qN$ against free-flow factor F for data of various investigators at Reynolds numbers above 300.

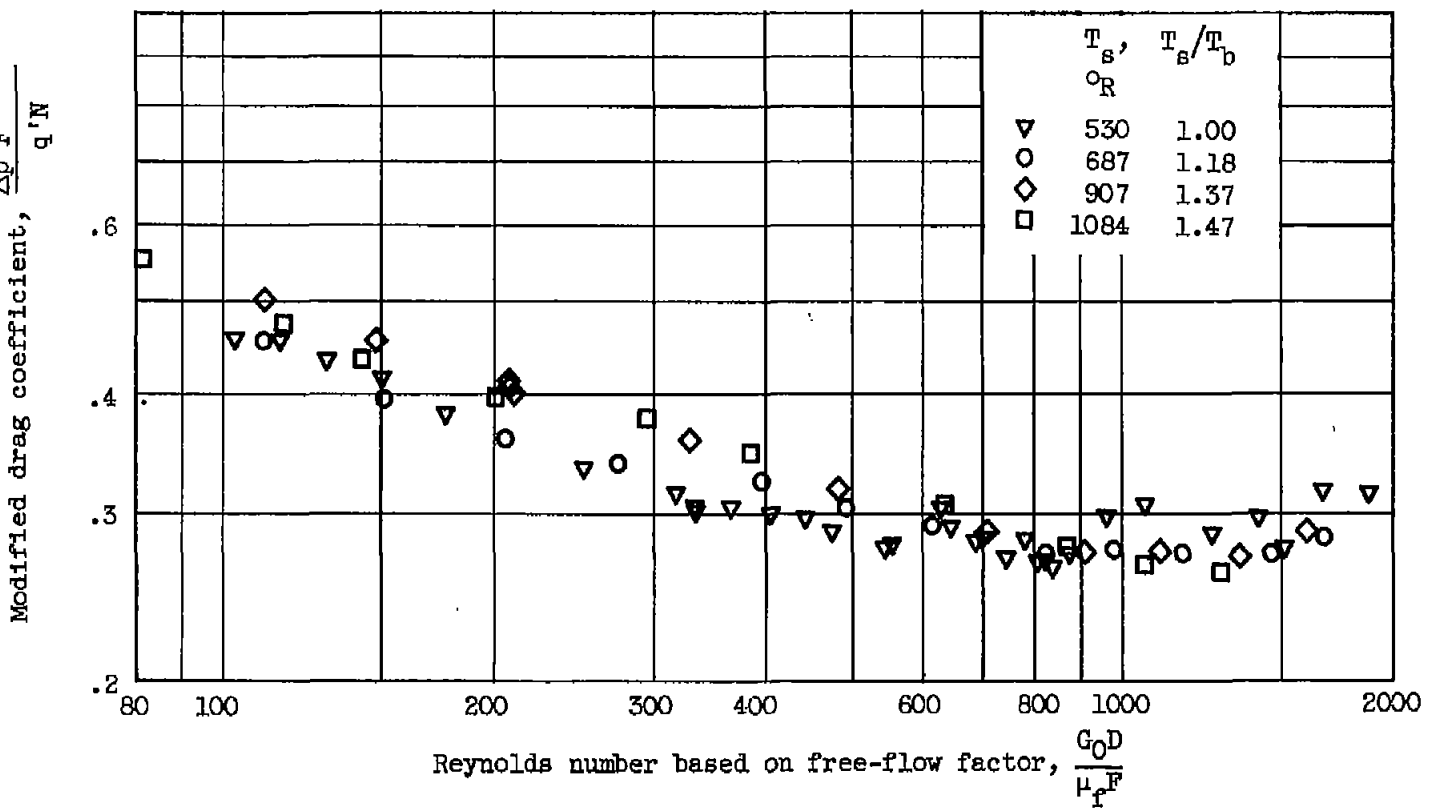

Figure 8. - Correlation of pressure-drop data.

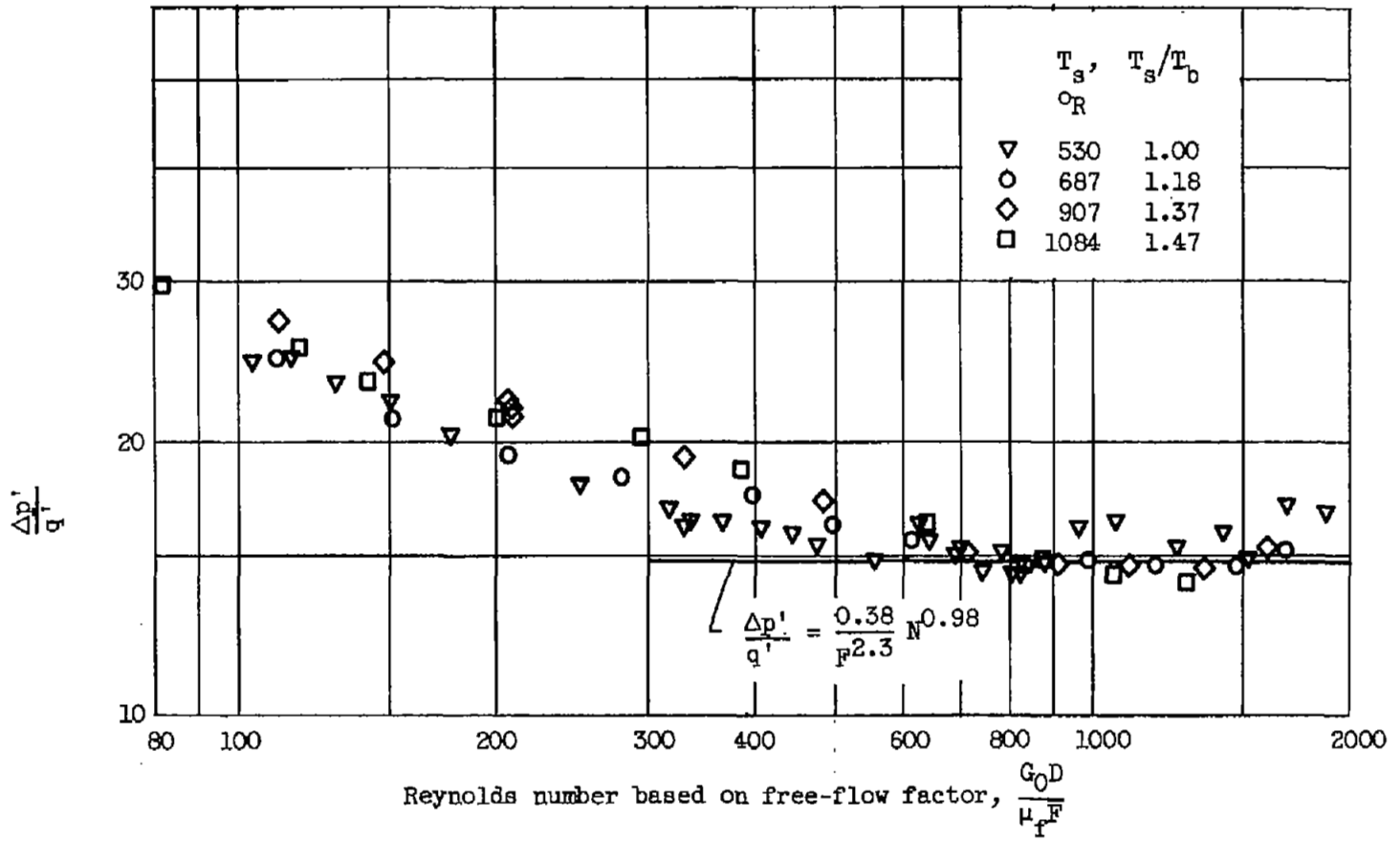

Figure 9. - Comparison of pressure-drop data.

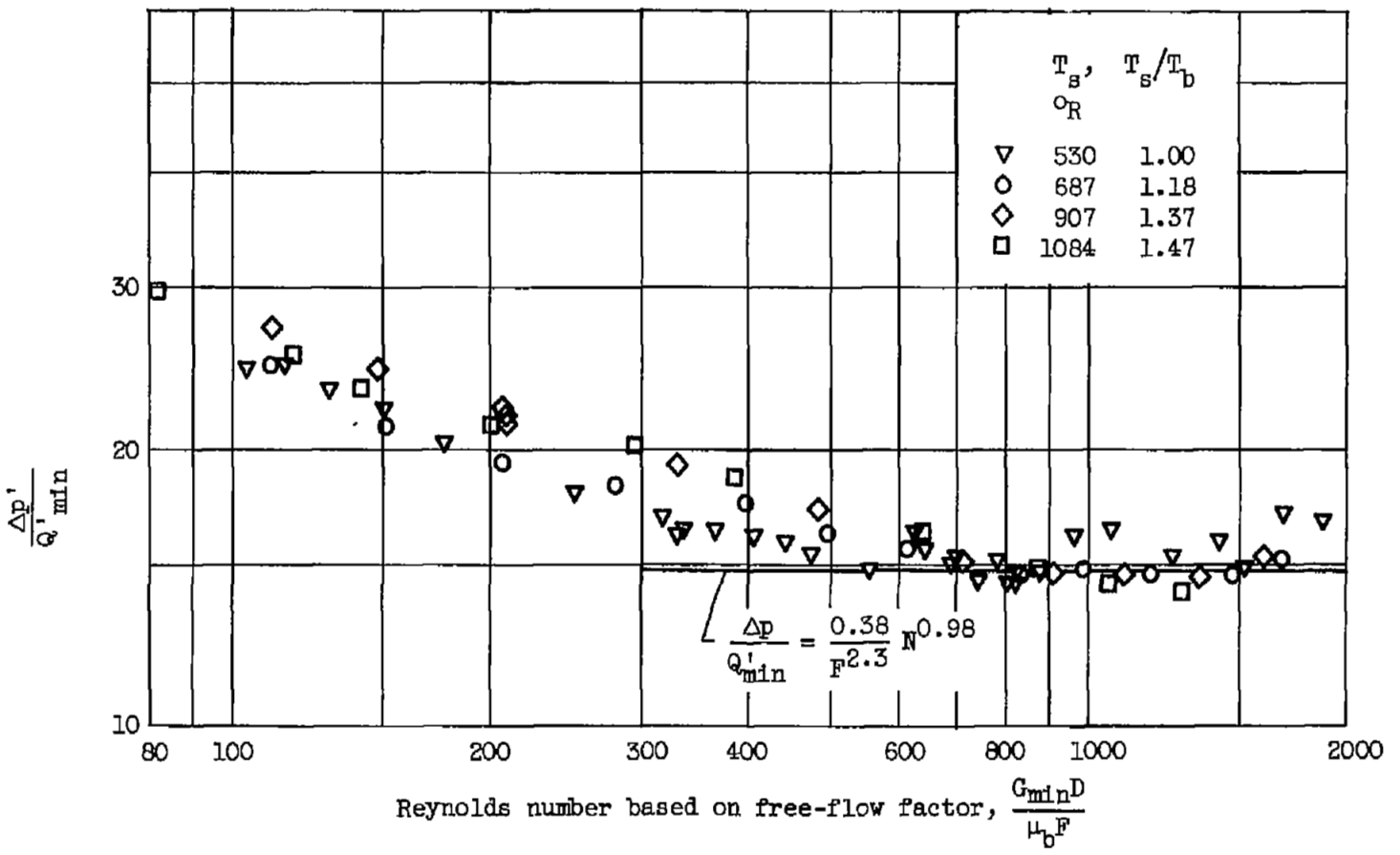

Figure 10. - Comparison of pressure-drop data.